Parolai, S., Bindi, D., Ansal, A., Kurtulus, A., Strollo, A., Zschau, J. (2010): Determination of shallow S-wave attenuation by down-hole waveform deconvolution: a case study in Istanbul (Turkey). - Geophysical Journal International, 181, 2, 1147-1158

DOI: 10.1111/j.1365-246X.2010.04567.x

Determination of shallow S-wave attenuation by down-hole waveform deconvolution: a case study in Istanbul (Turkey)

S. Parolai[1], D. Bindi[2], A. Ansal[3], A. Kurtulus[3] , A. Strollo[1,4], and J. Zschau[1]

[1]Deutsches GeoForschungsZentrum GFZ, Section 2.1, Telegrafenberg, 14473 Potsdam, Germany
[2]Istituto Nazionale di Geofisica e Vulcanologia, Via Bassini 15, 20133 Milano Italy
[3]Boğaziçi Üniversitesi, Kandilli Rasathanesi ve Deprem Araştırma Enstitüsü, Department of Earthquake Engineering, 34684, Çengelköy, Istanbul, Turkey
[4]Institute of Geosciences, Universität Potsdam, Karl-Liebknecht Strasse, 14476 Potsdam, Germany

Revised version

03-02-2010

Determination of shallow S-wave attenuation by down-hole waveform deconvolution: a case study in Istanbul (Turkey)

S. Parolai[1], D. Bindi[2], A. Ansal[3], A. Kurtulus[3], A. Strollo[1,4], and J. Zschau[1]

[1]Deutsches GeoForschungsZentrum GFZ, Section 2.1, Telegrafenberg, 14473 Potsdam, Germany
[2]Istituto Nazionale di Geofisica e Vulcanologia, Via Bassini 15, 20133 Milano Italy
[3]Boğaziçi Üniversitesi, Kandilli Rasathanesi ve Deprem Araştırma Enstitüsü, Department of Earthquake Engineering, 34684, Çengelköy, Istanbul, Turkey
[4]Institute of Geosciences, Universität Potsdam, Karl-Liebknecht Strasse, 14476 Potsdam, Germany

Abstract

The estimation of shear-wave velocity and attenuation in near-surface geology is of primary importance in engineering seismology. In fact, their knowledge is essential for site response studies when preparing improved seismic hazard scenarios. In this study, we propose two approaches for estimating the average shear-wave quality factor Qs by using recordings of a vertical array of accelerometers. The methods are mainly based on the deconvolution of the wavefield recorded in a borehole with that recorded at the surface.

The first method requires the Fourier transform of the deconvolved wavefield to be fitted with a theoretical transfer function valid for the vertical or nearly vertical (in the case at hand up to 30° incidence angle) propagation of S-waves. The second method is based on the spectral fitting of the Fourier transform of only the acausal part of the deconvolved wavefield with a theoretical transfer function.

Both methods can be applied without any prior knowledge of the subsoil structure (since they are based on empirical data analysis) and do not require a precise knowledge of the azimuthal orientation of the sensors in the boreholes (which is seldom available). First, we describe the theoretical framework of the proposed methodologies for Qs estimation, which are based on the assumption that the structure in the borehole is weakly heterogeneous in the vertical direction (that is, no large impedance contrast exists between the borehole sensor and the surface). Second, by using synthetic accelerograms, we verify that in a realistic subsoil structure, the assumption of vertical homogeneity can hold and we investigate the robustness and the suitability of the proposed methods. Finally, only the method that was shown to provide the more stable results, based on fitting the borehole-to-surface spectral ratio with a theoretical function, is applied to earthquakes signals recorded by a vertical array of accelerometers installed in Ataköy (western Istanbul). Results show that using borehole data provides a fair and robust estimate of an average Qs (of about 30, 46 and 99 for the 0-50, 0-70, 0-140 m depth ranges, respectively), that can be used for numerical simulations of ground motion.

Introduction

Near-surface material properties (e.g. shear wave velocity Vs and quality factor Qs) are useful parameters for improving seismic hazard assessment. Their estimation requires laboratory analysis of undisturbed samples and/or in situ measurements. While several recent studies in engineering seismology have focused on developing new methods for estimating in-situ S-wave velocity with good accuracy using both active (e.g. seismic refraction, seismic reflection, surface wave method, P-S logging) and passive source (seismic noise) methods, less attention has been dedicated to a reliable retrieval of attenuation in the near surface layers.

When boreholes are available, the quality factor can be estimated from vertical seismic profiling data (e.g. Tonn, 1991). The methods applied on the recorded data are generally based on spectral-ratio analysis (e.g. Gibbs et al., 1994; Parolai et al., 2007; Ge et al., 2009),

matching techniques (e.g. Raikes and White, 1984), spectral modeling, measurements of the amplitude decay in the time domain, synthetic modeling, rise time analysis, pulse amplitude method analysis (e.g. Tonn, 1991), and on the pulse width (Fletcher et al., 1990). The main drawback of using the spectral ratio is that it might be contaminated by multiples. In general, they can be eliminated if their corresponding elastic responses in the medium are known. Furthermore, the above described active-source based methods provide an estimation of Qs at frequencies much higher (generally >20 Hz) than those of primary interest to seismic hazard studies (roughly speaking between 0.1 and 10 Hz).

With regards to this, vertical arrays provide recordings of earthquake signals from different depths and at the surface, allowing, in principle, an in-situ estimation of the medium's characteristics over the frequency range of engineering interest. However, down going waves reflected at the surface might affect (especially for shallow boreholes) the downhole recordings. In this case, the simple spectral ratio method cannot lead to a robust estimation of Qs. In order to overcome this drawback, when possible (i.e. for a deep enough borehole sensor) the spectral ratio is taken between the up going and down going pulses in the downhole seismogram (e.g. Hauksson et al., 1987; Kinoshita, 2008). Alternatively, a fit can be carried out on the high-frequency part of the spectral ratio (f >20 Hz) which might be less affected by down going reflected phases (Aster and Shearer, 1991). Recently, Assimaki et al., (2008) proposed an inversion procedure that aims to estimate the best borehole model in term of shear wave velocity, attenuation and density, by optimizing the correlation between observed and synthetic seismograms. Under the condition that the orientation of the sensor is correctly known, the Qs might be estimated by an inversion procedure that optimizes the fit either between the observed and the calculated, for a certain model, amplitude spectral ratios (Seale and Archuleta, 1989) or between the observed and theoretical temporal propagator for a layered medium (Trampert et al., 1993).

In this paper we propose a new procedure for estimating the average Qs between the surface and a downhole sensor that does not require knowledge of the velocity structure in the downhole and is not dependent upon knowing the exact orientation of the sensors in the borehole. The procedure, which is based on the calculation of the deconvolved wavefield between the downhole and surface sensor (Mehta et al., 2007a; Parolai et al., 2009), allows us to identify and to model the effect of the down going waves, as well as to separate the contribution of up going and down going waves in the spectra of recordings collected by sensors installed in the borehole. The main assumptions of the method proposed here for estimating Qs are only that the impedance contrasts between soil layers in the investigated depth range are small (i.e. the main reflected pulse is only the one due to the free surface) and that the deconvolved wavefield is mainly dominated by a pulse corresponding to a nearly vertical propagation of plane S-waves. We first validate the method through synthetic data analysis and show that the method is able to provide a fair estimate of Qs that might be useful for site response analysis and synthetic seismogram calculations. Finally, we show an application to vertical array data from the Ataköy district of western Istanbul (Parolai et al., 2009).

Method

Following Safak (1997), if the input ground motion due to a vertical incident plane S-wave recorded at a borehole sensor at depth h is defined as $u(h; t)$, the motion $u(0; t)$ recorded at the surface in a homogeneous and elastic medium will be equal to $2u(h; t-\tau)$, where τ is the wave travel time from the depth h to the surface and the factor 2 accounts for the free surface effect. This value is appropriate for SH-waves but can vary for SV waves depending on the incidence angle and the Poisson ratio. The total motion recorded at the borehole sensors will therefore

be $u(h; t)+ u(h; t\text{-}2\tau)$, which accounts for the down going propagating wave reflected at the surface. Therefore, the transfer function $\tilde{S}(0,h;\omega)$ between the recording in the borehole and that at the surface, after having considered also anelastic effects and having taken their Fast Fourier Transform (FFT), can be written as:

$$\tilde{S}(0,h;\omega)=\frac{\tilde{U}(h;\omega)+\tilde{U}(h;\omega)e^{-2i\omega\tau}e^{(-\frac{\omega t}{Qs})}}{2\tilde{U}(h;\omega)e^{-i\omega\tau}e^{(-\frac{\omega t}{2Qs})}} \qquad (1)$$

Where $\tilde{U}(h,\omega)$ is the Fourier transform of the input motion at depth h.
The first exponential term in the second part of the numerator is related to the phase shift (travel time from bottom to top and vice versa) of the down going wave, while the second term takes into account the effect of attenuation through the quality factor Qs.
Similarly, the effect of propagation and attenuation from the bottom sensor to the surface is taken into account in the denominator. Again, the factor 2 accounts for the free surface effect.
Note that this equation is valid only for linear soil behavior.

The inverse Fourier transform of (1), $s(t)$, provides the deconvolved wavefield that clearly separates the contribution of the upgoing and down going waves:

$$s(t)=FFT^{-1}\left(\frac{\tilde{U}(h;\omega)+\tilde{U}(h;\omega)e^{-2i\omega\tau}e^{(-\frac{\omega t}{Qs})}}{2\tilde{U}(h;\omega)e^{-i\omega\tau}e^{(-\frac{\omega t}{2Qs})}}\right) \qquad (2)$$

The modulus of $\tilde{S}(0,h;\omega)$, after a few mathematical steps, is given by:

$$\left|\tilde{S}(0,h;\omega)\right|=\frac{\sqrt{1+e^{\frac{-4\pi f\tau}{Qs}}+2e^{\frac{-2\pi f\tau}{Qs}}\cos(4\pi f\tau)}}{2e^{\frac{-\pi f\tau f}{Qs}}} \qquad (3)$$

When recordings at the surface and at depth are available, the deconvolution of ground motion recorded at a depth h with that at depth 0 (free surface) can be written in the frequency domain as

$$\tilde{S}(0,h;\omega)=\frac{\tilde{B}(h;\omega)}{\tilde{Z}(0;\omega)} \qquad (4)$$

where $\tilde{Z}(0,\omega)$ and $\tilde{B}(h,\omega)$ are the Fourier transform of the motion recorded at the surface and at the depth h, respectively. However, the deconvolution operation is applied to data corrupted by noise and therefore, since this problem is ill-conditioned, small errors in the data could lead to solutions unacceptable from a physical point of view.
To avoid this instability, a regularized Tikhonov deconvolution can be used (Tikhonov and Arsenin, 1977; Bertero and Boccacci, 1998; Mehta et al., 2007b):

$$\tilde{S}_{\varepsilon}(0,h;\omega) = W_{\varepsilon}(\omega)\frac{\tilde{B}(h;\omega)}{\tilde{Z}(0;\omega)} \qquad (5)$$

where $\tilde{S}_{\varepsilon}(0,h;\omega)$ denotes the Fourier spectrum of the deconvolved wavefield and

$$W_{\varepsilon}(\omega) = \frac{|\tilde{Z}(0;\omega)|^2}{|\tilde{Z}(0;\omega)|^2 + \varepsilon} \qquad (6)$$

is the filter. ε refers to a positive constant added to the denominator to prevent the numerical instability of equation (4).

Starting from the similarity between deconvolution and the cross correlation tool used in seismic interferometry (amongst many others, see Lobkins and Weaver 2001; Schuster et al., 2004; Shapiro and Campillo 2004; Snieder et al., 2006; Halliday and Curtis, 2008), Mehta et al. (2007a; 2007b) and Parolai et al., (2009) showed that this approach is very efficient in providing useful insight into the wavefield propagation in the uppermost crustal layers. Moreover, they showed that independent of the chosen seismogram window, the deconvolved horizontal component wavefield is dominated by pulses propagating with velocities in agreement with the S-wave velocity structure of the site.

Method 1

In order to estimate the quality factor Qs, the modulus $\left|\tilde{S}_{\varepsilon}(0,h;\omega)\right|$ can be fitted by using equation (3) through a grid search procedure over Qs and τ.

The clear advantage of using the deconvolution of the motion at depth (with spectral troughs) with that at the surface is that the filter of equation (6) will not strongly affect the amplitude of the minima in the spectra of the deconvolved wavefield $\left|\tilde{S}_{\varepsilon}(0,h;\omega)\right|$. On the contrary, the spectral peaks in the standard spectral ratio surface-borehole would be strongly affected by regularization. In fact, the water level due to the introduction of ε would strongly affect the spectral troughs that would be at the denominator, therefore leading to more biased estimates of Qs.

Method 2

Alternatively, the acausal part of the deconvolved wavefield s(t) can be separated from the causal part. In this way, the FFT of the acausal part of the deconvolved wavefield $A(0,h;\omega)$ is not affected (see equation (1)) by the down going waves (generating troughs in the amplitude spectrum), with the amplitude spectral shape dependent on the term $0.5e^{\frac{\pi f\tau}{Qs}}$ (see equation 1 and 3). In this study, a grid search procedure is applied to Qs while τ is fixed to the value estimated by halving the time interval between the acausal and causal peaks in the deconvolved wavefield s(t) (Mehta et al., 2007a, 2007b; Parolai et al., 2009). Extending the grid search procedure also to this parameter would be possible.

Basic steps of the procedures

In this study, the deconvolution in equation (5) was carried out following Parolai et al.,(2009), fixing ε equal to 10% of the average spectral power of $\tilde{Z}(0,\omega)$. Furthermore, while applying method 1, the grid search was carried out with Qs values ranging between 1 and 500 with steps of 1. τ was also inverted in the grid search procedure in order to take into account

uncertainties in its measurements, with a range of values spanning +/- two time samples around the estimated value. The misfit was evaluated as the root mean square of the differences between the logarithm of the observed and calculated deconvolved-wavefield amplitude spectra.
The grid search in method 2 was carried out using the same Qs range and step as in method 1. τ was fixed to the value estimated by halving the time interval between the acausal and causal peaks in the deconvolved wavefield s(t) obtained by the FFT^{-1} of $\tilde{S}_{\varepsilon}(h,0;\omega)$
The free surface effect related parameter *a,* that in the definition of equation (1) was fixed equal to ½ (see Method 2 description), was also considered as a free parameter, with it set to vary between 0.01 and 1, with steps of 0.01. Although, test we carried out (here not shown) have indicated that for the a wide range of incidence angle (up to 30°) and realistic Poisson ratio for the investigated site (see Table 1) its values will not deviate significantly from 0.5, we decided to leave free this parameter in the grid search procedure to account for incidences slightly different from the normal one. The misfit was evaluated as the root mean square of the differences between the observed and calculated amplitude spectra of the acausal part of the deconvolved wavefield.
In this study, Qs was assumed to be frequency independent in agreement with standard engineering practice. However, a modification to method 1 that would allow it to take into account frequency dependence would be possible. In such a case, Qs might be expressed as $Qs(f)=Q_0 f^{\beta}$, where *f* indicates the frequency, and the grid search procedure could also be carried out for Q_0 and β. However, the frequency dependence of the quality factor is still an open issue (e.g. Morozov, 2008).

Validation with synthetic data

The suitability of the proposed method to provide reasonable estimations of average Qs over the investigated depth interval was evaluated by means of numerical simulations. Synthetic seismograms were calculated using a layered subsoil velocity model derived for the vertical array in Ataköy (Parolai et al., 2009) by means of seismic noise array data analysis (e.g. Aki, 1957; Okada, 2003; Parolai et al., 2005; Parolai et al., 2006). This model was shown to provide deconvolved wavefield pulse arrivals consistent to those observed with real data. The quality factors for P- and S-waves, as well as the density values, were not available. Therefore, they were assigned values suitable for near-surface soft geological material. The synthetic seismogram calculations were carried out using a viscoelastic matrix propagator method (Wang, 1999), with the source at a depth of 10 km. Since the deconvolution results are not expected to depend on the chosen source, we selected arbitrarily a fault plane with a strike, dip and rake of 94°, 90°, and 56°, respectively. The model is described in detail in Table 1, and the uppermost structure (0-160 m depth range) is shown in Figure 1.

[Figure 1]

The synthetic seismograms were calculated for the radial and transverse components of motion for depths of 0, 50, 70 and 140 m, corresponding to the installation depths of the accelerometers in the Ataköy vertical array. In order to be consistent with the application to the real data of Parolai et al., (2009) which will be carried out in the following section, the seismograms were first derived to obtain acceleration, and then a single horizontal component for each depth was calculated by means of rotation in the direction that determines the maximum spectral energy. Furthermore, the amplitudes of maximum horizontal accelerations were first scaled to be consistent with values recorded in the Ataköy vertical array and then

added to real noise recorded simultaneously at the corresponding depths. Finally, the deconvolved wavefields were calculated by applying equation (5) to the synthetic data.
The obtained synthetic accelerations and the deconvolved wavefields are shown in Figure 2.

[Figure 2]

This figure shows, consistent with the results for the real data of Parolai et al., (2009), that although the medium is layered, due to the small impedance contrasts between the layers, the deconvolved wavefield is dominated by an up going and down going wave generated by free-surface reflection. This supports the initial hypothesis that method 1 and 2 can be still reasonably applied if the model is not fully homogeneous.

Results: Method 1
The FFT of the deconvolved wavefield was calculated and fitted by the grid search procedure described above using equation (3). The frequency band on which the spectral fit was carried out (1-15 Hz for the 0-50 m and 0-70 m depth intervals, and 0.6-15 Hz for the 0-140 m depth interval) was selected after a visual inspection. The results from the test that we carried out, however, showed a very weak dependence on the chosen frequency band. Figures 3, 4 and 5 show the grid search results for the deconvolved wavefields between 50, 70 and 140 m depth and the surface, respectively. The color scale indicates the misfit values (blue, small and red, large) obtained for couples of Qs and τ. It is worth noting that the lower bound of the quality factors yielding fair fits to the deconvolved wavefields (see the details in the bottom panels) is quite clearly determined by the rapid increase of the slope of the misfit function towards lower Qs values. On the other hand, the increase of misfit is much less steep toward higher values of the quality factor, therefore indicating a larger uncertainty in defining an upper limit. This trend was expected considering the chosen misfit function.

[Figure 3]
[Figure 4]
[Figure 5]

For the depth interval 0-50 m the best fit is obtained for Qs=15, which is between the values of 10 and 20 encountered over this depth range, and a τ value of 0.139 s. Figure 6 (top), shows that the values provided by the grid search procedure allow an excellent fit of the deconvolved wavefield amplitude spectra.
For the depth ranges 0-70m and 0-140 m (Figures 4 and 5), the averaged Qs values obtained are 15 and 27, respectively. Both values lie between the values encountered in these depth ranges and, importantly, the average Qs estimated increases when widening the investigated depth range, consistent with the increase of Qs with depth in the adopted model. The low average Qs values (with respect to the Qs of the layer in which the sensor was located) for the largest depth range is consistent with a dominance in the average Q determination of the slow paths in the shallowest (and more attenuating) layers. However, we noticed that when broadening the depth range, the misfit increases. Comparing the deconvolved wavefield amplitude spectra with those calculated by equation (3) and using the minimum misfit parameters (Figure 6) confirms that a larger mismatch between observed and fitted data exists when increasing the depth of the borehole sensor. This is due to the fact that broadening the investigated depth interval implies including additional layering into the model and therefore weakening the starting assumption of vertical homogeneity.
Moreover, the analysis of the deconvolution of the surface wavefield with itself showed that the effect of the filter of equation (6) becomes stronger below 2 Hz, leading to smaller

spectral amplitudes. This might explain the differences between the synthetic deconvolved wavefield and the calculated minimum misfit parameter spectral amplitude.
Finally, we investigated if constraining the grid search procedure to fit the first low-frequency trough might still lead to small misfit models that we might have overlooked. Regarding this point, first, a close inspection of a wider area of the misfit function revealed no other global minimum. Second, a visual inspection of the deconvolved wavefield spectral amplitude determined with the minimum misfit parameter obtained under this extra constraint showed a clear augment of the misfit. In particular, troughs at higher frequencies were not fitted at all.

[Figure 6]

Results: Method 2
The spectral fit was carried out, as described above, using a grid search procedure. The 2-20 Hz frequency band was chosen for these calculations since, as shown by the spectrum of the surface wavefield deconvolved with itself in Figures 7, 8, and 9, the filter in equation (6) is affecting the amplitude by less than 20% of their values. Furthermore, a nearly linear trend is observed in the $A(0,h;\omega)$ spectrum when plotted on a lin-log scale, showing that most of the effect of the surface reflected down going wave was removed. Scattering of the spectral amplitudes and small spectral troughs at 16 Hz, 12 Hz, and 8 Hz at 50, 70 and 140 m depths, respectively, might be due to down going waves being reflected at the layer boundaries (Trampert et al., 1993; Parolai et al., 2009).

[Figure 7]
[Figure 8]
[Figure 9]

The results in Figures 7, 8 and 9 show that, in general, some trade-off between the Qs and a (the free-surface effect) exists. Average Qs were estimated to be 18, 13 and 20 for the 50, 70 and 140 m depth ranges, respectively, while the surface effect a was estimated to be 0.49, 0.45 and 0.38 for the 50, 70 and 140 m depth ranges, respectively. Although the average quality factor values represent reasonable approximations of the Qs encountered in these depth ranges, the lack of increase in Qs when broadening the investigated depth range between 50 and 70 m is worthy of attention and might indicate some weaknesses in the proposed procedure. In fact, contrary to what we observed for method 1, repeating the fit while changing slightly the exploited frequency band lead to very large variability in the results. For example, selecting a 2-15 Hz frequency band lead to an average Qs=22 for the depth range 0-50 m, a value even larger than the Qs assumed for the model layers (see Table 1). Attempts to estimate Qs via a linear fit of the natural logarithm of the spectral amplitudes of $A(0,h;\omega)$ lead to even worse results due to the higher degree of freedom of the used linear function that might also allow negative Qs. Since these problems arise and worsen when analyzing real data affected by more noise (also due to more complicated shallow geology with respect to the synthetic models), when the undulating behavior of the spectral amplitudes with frequency makes the fit strongly dependent on the chosen frequency band, in this study we decided to adopt only method 1 for the estimation of an average Qs factor from the Ataköy vertical array data.

Reliability test
In order to validate if the average Qs estimated by method 1 provides a fair representation of the attenuation that affects S-waves during their propagation through the investigated depth range, we carried out numerical simulations using the model described in Table 1, but

substituting for the starting Qs values the average Qs. That is, we used a constant Qs equal to 15, 15 and 27 for the depth ranges 0-50 m, 0-70 m and 0-140 m, respectively.
We calculated the synthetic seismograms corresponding to the transverse component of ground motion, since they depend only on Qs, and we compare them to those calculated for the model in Table 1. The comparison is carried out in terms of the squared coherency calculated between the seismograms estimated using the complex multitaper spectral coherence as proposed in Mann and Park (1993), Lall and Mann (1995) and Mann et al., (1995). Multitaper methods offer the opportunity to compute the coherence by applying some kind of time-frequency ensemble, using the FFT of the considered seismograms tapered with a certain taper. Tapers are constructed to minimize the spectral leakage outside a chosen central bandwidth. The optimal tapers belong to a family of functions known as discrete prolate spheroidal sequences. For this analysis, five 3π-prolate tapers were used as a compromise between spectral resolution and variance. Note that a small number of π increases the low frequency resolution, but can lead to peak splitting in the high-frequency range. For a comparison, synthetic seismograms and the respective squared coherency were also calculated for each depth range, adopting average Qs values lower and higher than those leading to the minimum misfit. Figures 10, 11 and 12 show that the level of coherency is generally very high (>0.992). This result is not surprising since only the Qs factor was changed while performing the numerical simulation.
Figure 10 shows the results when the 0-50 m depth range is considered. The minimum misfit average Qs clearly shows a higher coherency than the other considered values. Moreover, the figure highlights that for the whole analyzed frequency band (when the energy of the signal is larger) the average Qs allows a fair calculation of the spectral amplitude. Extending the analysis to other average Qs values allows us to note that average Qs values between 10 and 15 might even provide better squared coherency values than Qs=15. We believe that this small discrepancy between our minimum misfit estimate and values yielding to the highest coherency in the signals might be due to the approximation we made in describing propagation in the borehole simply by equation (1). Nevertheless, Figure 10 clearly confirms the appropriateness of the estimated average Qs in describing energy losses in the 0-50 m depth range.
Similar results were obtained for the 0-70 m and 0-140 m depth range (Figures 11 and 12). However, the diminishing of the squared coherency values for the minimum misfit Qs when increasing the depth range confirms that broadening the investigated depth interval implies including additional layering and heterogeneities, therefore increasing the disagreement with the assumptions for the model in equation (1).

[Figure 10]
[Figure 11]
[Figure 12]

Application to real data: the Ataköy vertical array

In December 2005, a drilling program consisting of four boreholes of 25m, 50 m, 70 m and 140 m deep was realized (ZETAŞ®, 2006) in western Istanbul (Turkey) in the district of Ataköy (Figure 13). PVC pipes were installed in the borehole and the space between the piping and boreholes was filled with cement grout. Within the 140 m deep borehole, based on the encountered subsoil conditions, representative and/or undisturbed soil samples were obtained and Standard Penetration Test (SPT) carried out at regular intervals of 1.5 m. The water table was encountered at 15 m depth.

[Figure 13]

The array was instrumented with 3 Shallow Boreholes accelerometers (SBEPI) at 25, 50 and 70 m depth and a Down borehole accelerometer (ES-DH) at 140 m depth, connected to a 12 channel K2 at the surface. Additionally, a K2 with internal episensor was installed at the surface. A total of 60 SPT samples and 3 undisturbed samples (from depths 35 m, 49 m, and 52 m) were chosen for laboratory tests, including sieve analysis, with the aim of estimating natural moisture content and Atterberg's limits.

Within the first 15 meters depth, the subsoil is composed of light brown, hard gravelly sandy clay. Below this layer, limestone with a low Rock Quality Designation (RQD) and clay interlayers were found down to 35 meters depth. Below this depth until the bottom of the deepest borehole, hard/very dense sandy clay/clayey sand layers were encountered.

In addition, in order to estimate the S-wave velocity profile at the vertical array site, both PS Logging (Nigbor and Imai, 1994) as well as micro array measurements of noise (e.g. Aki, 1957; Okada, 2003) were carried out. For the latter, an array of 12 stations was installed in the vicinity of the vertical array installation, and the data were analyzed and inverted following Ohori et al., 2002; Parolai et al., 2005; Picozzi et al., 2005; Parolai et al., 2006). The S-wave velocity profile at the vertical array site is shown in Table 1 and Figure 1. More details about the soil structure and the performed investigations are given in Parolai et al., (2009). Figure 13 shows an example of the recordings made by the vertical array of a M=4.6 event which occurred on March 12 2008 (see Table 1 in Parolai et al., 2009 for further details).

In this study, we apply method 1 to the horizontal component wavefield deconvolution results of Parolai et al., (2009) (their Figure 12). We did not consider the deconvolution results obtained for the 25 m depth accelerometer because it records ground acceleration values systematically smaller than those recorded at the surface and at 50 m depth. Since it is not possible, based on our knowledge of the subsoil structure, to justify such an observation, it is believed that the lower amplitude level recorded might be due to the insufficient coupling of the sensor which would therefore bias the Qs estimate.

The $\left|\tilde{S}_{\varepsilon}(0,h;\omega)\right|$ curves obtained by the real data analysis (Figure 14) clearly show similarities with those derived from our synthetic data simulation. In particular, clear spectral troughs appear at well-defined frequencies, with the first trough occurring at lower frequencies when increasing the depth range investigated. The number of troughs also increases when broadening the depth range due to the effect of higher harmonics.

[Figure 14]

Figure 15, 16 and 17 show the results obtained after applying method 1. Although larger uncertainties appear with respect to the synthetic data analysis (due to the complicated real earth structure with respect to the simplified, although realistic, model) a fair estimate of Qs is possible for all three investigated depth range. Similarly to the analysis with synthetic data, the lower bound of the fair average Qs values is better defined than the upper one. Moreover, interestingly, this lower bound, as well as the minimum misfit Qs, shifts to higher values when the investigated depth range is broadened. The average Qs obtained are 30, 46 and 99 for the 0-50, 0-70, 0-140 m depth ranges, respectively. The larger average Qs values derived by real data with respect to those adopted in the numerical simulations could have been expected when comparing the stronger attenuation influencing the causal peaks in Figure 2 (compare the relative amplitudes of the causal and acausal peaks) with respect to that occurring for the real data causal peak in Figure 12 in Parolai et al., (2009).

Finally, Figure 14 shows that a satisfactory fit of the curves calculated by equation (3) is obtained when using the average Qs values estimated by the grid search procedure.

[Figure 15]
[Figure 16]
[Figure 17]

Unfortunately, our estimates cannot be compared with Qs values calculated using other geophysical methods. Moreover, the few existing relationships between S-wave velocity and Qs that can be found in literature show a large scatter and significant differences amongst them. Therefore, they cannot be used to validate our results. Nevertheless, we calculated average Qs values for the vertical array in Ataköy starting from the measured S-wave velocities using the equation proposed by Wang et al., (1994) and Brocher, (2008) We obtained Qs values of 16 and 34, 18 and 35, 22 and 41, for the depth range 0-50 m, 0-70 m and 0-140 m, respectively. Note that the values obtained by Wang et al., (1994) have an uncertainty of ±12. In general, there is good agreement, especially in the 0-50 m and 0-70 m depth range, between our estimates based on equation (3) and those derived by the empirical relationships. Note that the discrepancies seem to increase with increasing analysis depth range. We remind the reader that the uncertainties in our estimations based on equation (3) increase with widening the investigated depth range. Based on this consideration and on the reliability test results we believe that our Qs estimates can be considered a fair approximation of the average Qs in Ataköy.

Conclusions

In this work, we proposed two methods for estimating the average quality factor Qs using recordings available from a vertical array. Both methods are based on the spectral analysis of a seismogram recorded at a given depth deconvolved, with the seismograms recorded at the free surface. In particular, the first method is based on fitting the full deconvolved wavefield with a theoretical model, whereas in the second method, the causal part of the propagator, corresponding to only the up-going propagation, is first isolated and then considered for the fitting procedure. Both methods have the advantage of not requiring any a-priori knowledge of the structure below the site. Moreover, a good knowledge of the azimuthal orientation of the sensors within the boreholes is not mandatory. In fact, previous studies (e.g. Parolai et al., 2009) showed that the deconvolved wavefield is dominated by a pulse propagating with a velocity consistent with that of plane S-waves propagating vertically. The major limitation involves the theoretical model considered in this work for the spectral fitting, which is valid only for nearly vertical propagation in a homogeneous medium. Therefore, we first assessed the suitability of the two methods by performing tests with synthetic data, but generated considering the model previously derived for the Ataköy vertical array (western Istanbul). Although increasing the depth of investigation causes the fit between the modeled and observed data to worsen, due to the limitation in the method that does not consider a layered model, the average Qs values estimated were found to be a fair representation of the Qs encountered by seismic waves while propagating from the borehole sensor to the surface. Moreover, the first method provided results more stable with respect to the frequency band selected for performing the spectral fitting, hence it was preferred for the analysis of actual data. Since the tests with synthetic data showed that reliable results can also be obtained when the model is not homogeneous (although without sharp velocity contrasts), we applied the first method to data recorded at the Ataköy vertical array to estimate the average quality factor over different depth ranges that might be considered in numerical simulations for seismic hazard studies.

In the future, we will attempt to improve the procedure by taking into account the existence of vertical velocity discontinuities in the sub-soil.

Acknowledgements
We thank the Associated Editor A. Curtis, Kurang Mehta and an anonymous reviewer for the comments and suggestions that helped in improving the manuscript. D. Bindi participated to this study during a visiting period at the GFZ. R. Milkereit improved the figures. K. Fleming kindly improved our English. The figures were generated using GMT (Wessel and Smith, 1991).

References

Aki, K. (1957). Space and time spectra of stationary stochastic waves, with special reference to microtremors. *Bull. Earthq. Res. Inst.* **35**, 415-456.

Assimaki, D., W. Li, J. H. Steidl, and K. Tsuda (2008), Site amplification and attenuation via downhole array seismogram inversion: a comparative study of the 2003 Miyagi-Oki aftershock sequence. *Bull. Seism. Soc. Am.* **98**, 301-330.

Aster R.C., and P.M. Shearer (1991). High-frequency borehole seismograms recorded in the San Jacinto fault zone, Southern California part 2. attenuation and site effects. *Bull. Seism. Soc. Am*. **81**, 1081-1100.

Bertero, M. and P. Boccacci (1998). Introduction to inverse problems in imaging. Bristol:IOP Publishing.

Brocher T.M. (2008). Compressional and Shear-wave velocity versus depth relations for common rock types in northern California. *Bull. Seism. Soc. Am*. **98**, 950-968.

Fletcher J.B., T. Fumal, H.-P. Liu, and L. Carroll (1990). Near-surface velocities and attenuation at two boreholes near Anza, California, from logging data. *Bull. Seism. Soc. Am*. **80**, 807-831.

Ge, J., J. Pujol, S. Pezeshk, and S. Stovall (2009). Determination of shallow shear-wave attenuation in Mississippi embayment using vertical seismic profiling data. *Bull. Seism. Soc. Am*. **99**, 1636-1649

Gibbs, J.F., D. M. Boore, W.B. Joyner, and T. E. Fumal (1994). The attenuation of seismic shear waves in Quaternary alluvium in Santa Clara Valley, California. *Bull. Seism. Soc. Am*. **84**, 76-90.

Halliday D., and A. Curtis (2008). Seismic interferometry, surface waves and sources distribution. *Geophys. J. Int.*, **175**, 1067-1087, doi:10.111/j.1365-246X.2008.03918.x

Hauksson E., T.-L. Teng, and T. L. Henyey (1987). Results from a 1500 m deep, three-level downhole seismometer array: site response, low Q values and fmax. *Bull. Seism. Soc. Am*. **77**, 1884-1904.

Kinoshita S. (2008). Deep-borehole-measured Qp and Qs attenuation for two Kanto sediment layer sites. *Bull. Seism. Soc. Am*. **98**, 463-468.

Lall, U., and M. Mann (1995). The Great Salt Lake: a barometer of low-frequency climatic variability. *Water Resour. Res*., **31**, 2503-2515.

Lobkins, O.I., and R.L. Weaver (2001). On the emergence of the Green's function in the correlation of a diffuse field. *Journal of Acoustical Society of America*, **110**, 3011-3017.

Mann, M. E., and J. Park (1993). Spatial correlation of interdecadal variation in global surface temperatures. *Geoph. Res. Lett.* **20**, 1055-1058.

Mann, M.E., U. Lall, B. Saltzman (1995). Decadal-to-centennial-scale climate variability: insights into the rise and fall of the Great Salt Lake. *Geoph. Res. Lett.* **22**, 937-940.

Mehta, K., R. Snieder, and V. Grazier (2007a).Extraction of near-surface properties for a lossy layered medium using the propagator matrix. *Geophys. J. Int*., **169**, 2171-280.

Mehta, K., R. Snieder, and V. Grazier (2007b). Downhole receiver function: a case study. *Bull. Seism. Soc. Am*. **97**, 1396-1403.

Morozov,I.B. (2008). Geometrical attenuation, frequency dependence of Q, and the absorption band problem. *Geophys. J. Int*., **175**, 239-252.

Nigor, R. L., and T. Imai (1994). The suspension P-S velocity logging method. *Proc. XIII International Conference on Soil Mechanics and Foundation Engineering*, 5-10, January 1994, New Delhi, India.

Ohori, M., A. Nobata, and K. Wakamatsu (2002). A comparison of ESAC and FK methods of estimating phase velocity using arbitrarily shaped microtremor analysis. *Bull. Seism. Soc. Am.* **92**, 2323-2332.

Okada, H. (2003). The microtremor survey method. *Geophysical monograph series* **12**, American Geophysical Union, Washington

Parolai, S., M. Picozzi, S. M. Richwalski, and C. Milkereit (2005). Joint inversion of phase velocity dispersion and H/V ratio curves from seismic noise recordings using a genetic algorithm, considering higher modes. *Geoph. Res. Lett.* **32**, L01303, doi: 10.1029/2004GL021115.

Parolai S, S.M. Richwalski, C. Milkereit, and D. Faëh (2006). S-wave velocity profiles for earthquake engineering purposes for the Cologne area (Germany). *Bull Earth. Eng.* **4**, 65–94.

Parolai, S., M. Mucciarelli, R. Gallipoli, S.M. Richwalski, and A. Strollo (2007). Comparison of Empirical and Numerical Site Responses at the Tito Test Site, Southern Italy. *Bull. Seism. Soc. Am*. **97**, 1413-1431.

Parolai, S., A. Ansal, A. Kurtulus, A. Strollo, R. Wang and J. Zschau (2009). The Ataköy vertical array (Turkey): insights into seismic wave propagation in the shallow-most crustal layers by waveform deconvolution. *Geophys. J. Int*. doi:10.1111/j.1365-246X.2009.04257.x

Picozzi, M., S. Parolai, S. Richwalski, (2005). Joint inversion of H/V ratios and dispersion curves from seismic noise: Estimating the S-wave velocity of bedrock. *Geophysical Research Letters*, **32**, 11, L11308, doi: 10.1029/2005GL022878.

Raikes S.A., R.E. White (1984). Measurements of earth attenuation form downhole and surface seismic recordings. *Geophysical Prospecting* **32**, 892-919.

Safak, E. (1997). Models and methods to characterize site amplification from a pair of records. *Earthquake Spectra*, EERI **13**, 97-129.

Schuster, G.T., J. Yu, J. Sheng and J. Rickett (2004). Interferometric/daylight seismic imaging. *Geophy. J. Int.*, **157**, 838-852.

Seale, S. and R. Archuleta (1989). Site amplification and attenuation of strong ground motion, *Bull. Seism. Soc. Am*. **79**, 1673-1696.

Shapiro, N.M and M. Campillo (2004). Emergence of broadband Rayleigh waves from correlations of ambient seismic noise. *Geophys. Res. Lett*., **31**, L07614,doi10.1029/2004GL019491.

Snieder, R., J. Sheiman and R. Calvert (2006). Equivalence of the virtual-source method and wave-field deconvolution in seismic interferometry. *Physical Review E*, **73**, 066620.

Tikhonov, A.N. and V.Y. Arsenin (1977). Solution of ill-posed problems. Washington:Wiston/Wiley.

Tonn, R. (1991). The determination of seismic quality factor A from VSP data: a comparison of different computation methods. *Geophysical Prospecting* **39**, 1-27.

Trampert, J., M. Cara, and M. Frogneux (1993). SH propagator matrix and Qs estimates from borehole- and surface-recorded earthquake data, *Geophy. J. Int*. **112,** 290-299**.**

Wang, R., (1999). A simple orthonormalization method for stable and efficient computation of Green's functions. *Bull. Seism. Soc. Am*. **89**, 733-741.

Wang, Z., R. Street, and E. Woolery (1994). Qs estimation for unconsolidated sediments using first-arrival SH wave critical refractions. *Journal of Geophysical research*, **99**, 13.543-13.551.

Wessel, P., and W.H.F. Smith (1991). Free software helps map and display data. *EOS Trans. AGU* **72**, 441, 445-446.

ZETAŞ® (2006). Factual report on drilling for strong ground motion network, 03/04/2006. ZETAŞ® Zemin Teknolojisi A.Ş.

Figure Captions:

Figure 1: a) The P- (dashed line) and S-wave (continuous line) velocity profiles determined at the Ataköy vertical array by Parolai et al. (2009) used in the numerical simulations. Triangles indicate the accelerometer positions. b) The Qp (dashed line) and Qs (continuous line) variation with depth in the subsoil model used for the numerical simulations. Triangles indicate the accelerometer positions. Note that data recorded by the accelerometer installed at 25 m depth were not used in the analysis (see the text for an explanation).

Figure 2: (Left) Synthetic maximum horizontal component accelerations for different depths (see Table 1). The insets show windows of pre-event noise in order to highlight their different amplitudes, consistent with their different depth of recording. (Right) Deconvolved wavefield for 50, 70 and 140 m depth, obtained by using equation (5).

Figure 3: a) Grid search results for the depth interval 0-50 m for Method 1. The white triangle indicates the position of the minimum misfit. The gray line indicates the position of a cross-section of the misfit function passing through the global minimum. The color scale indicates the misfit values obtained with the grid search procedure. Qs values ranging between 1 and 500 with steps of 1, and τ spanning +/- two time samples around the estimated value with steps of 0.00007 sec were inverted in the grid search procedurę. b) Cross-section of the misfit function (gray line in the top panel). The red triangle indicates the position of the minimum. The inset is a zoom of the area within the gray rectangle.

Figure 4: As in Figure 3, but for the depth interval 0-70 m.

Figure 5: As in Figure 3, but for the depth interval 0-140 m.

Figure 6: Synthetic acceleration deconvolved wavefield amplitude spectra (black) and calculated deconvolved wavefield spectra using the minimum misfit parameters (gray). Results are shown, from top to bottom, for the 0-50 (a), 0-70 (b) and 0-140 m (c) depth ranges.

Figure 7: a) Grid search results for the depth interval 0-50 m for Method 2. The white triangle indicates the position of the minimum misfit. Qs values ranging between 1 and 500 with steps of 1, and a ranging between 0.01 and 1, with steps of 0.01 were inverted in the grid search procedure. b) Spectral amplitude of the surface wavefield deconvolved with itself (black points) and of $A(0,50;\omega)$ (gray points). The minimum misfit solution is indicated by the red line.

Figure 8: As in Figure 76, but for the depth range 0-70 m.

Figure 9: As in Figure 7, but for the depth range 0-140 m.

Figure 10: Multitaper squared coherency $|C(f)|^2$ estimates between the transverse component seismogram generated using the model in Table 1 and those calculated using an average Qs value (black line) over the 0-50 m depth range. The associated standard deviation uncertainties are indicated by the gray area. Results for an average Qs=5 (a), Qs=15 (b) and Qs=30 (c) are shown.

Figure 11: As in Figure 10, but for the 0-70 m depth range. The associated standard deviation uncertainties are indicated by the gray area. Results for an average Qs=5 (a), Qs=15 (b) and Qs=30 (c) are shown.

Figure 12: As in Figure 10, but for the 0-140 m depth range. The associated standard deviation uncertainties are indicated by the gray area. Results for an average Qs=10 (a), Qs=27 (b) and Qs=50 (c) are shown.

Figure 13: a) Map of the area under investigation. The triangle shows the location of the vertical array. b) Accelerometric recordings by the vertical array stations of the 18:53:38.5 March 12 2008 M=4.6 earthquake, which occurred at latitude 40.84° and longitude 28.99°. The hypocentral depth was estimated to be 10 km. More details about the recordings can be found in Parolai et al., (2009).

Figure 14: Observed acceleration deconvolved wavefield amplitude spectra (black) and calculated deconvolved wavefield spectra using the minimum misfit parameters (gray). Results are shown, from top to bottom, for the 0-50 m (a), 0-70 m (b) and 0-140 m (c) depth ranges.

Figure 15: a) Grid search results on the observed data for the depth interval 0-50 m for Method 1. The white triangles indicate the position of the minimum misfit. The gray line indicates the position of a cross-section of the misfit function passing through the global minimum. . Qs values ranging between 1 and 500 with steps of 1, and τ spanning +/- two time samples around the estimated value with steps of 0.0002 sec were inverted in the grid search procedure .b) Cross-section of the misfit function (gray line in the top panel). The red triangle indicates the position of the minimum. The inset is a zoom of the area within the gray rectangle.

Figure 16: As in Figure15, but for the depth range 0-70 m.

Figure 17: As in Figure15, but for the depth range 0-140 m.

Table 1: Model parameters used in the synthetic seismogram generation, based on the inferred velocity model for the Ataköy district of western Istanbul (see Parolai et al., 2009).

No	Thickness (m)	Vp (m/s)	Vs (m/s)	Density (g/cm^3)	Qp	Qs
1	19	700	350	1.8	30	10
2	24	1400	330	1.9	30	10
3	35	1500	444	1.9	50	20
4	34	1600	596	1.9	100	50
5	40	1700	689	1.9	200	100
6	72	1750	728	1.95	300	150
7	109	1800	684	2.0	300	150
8	3167	2250	982	2.3	400	200
9	Standard crustal model					

Figures

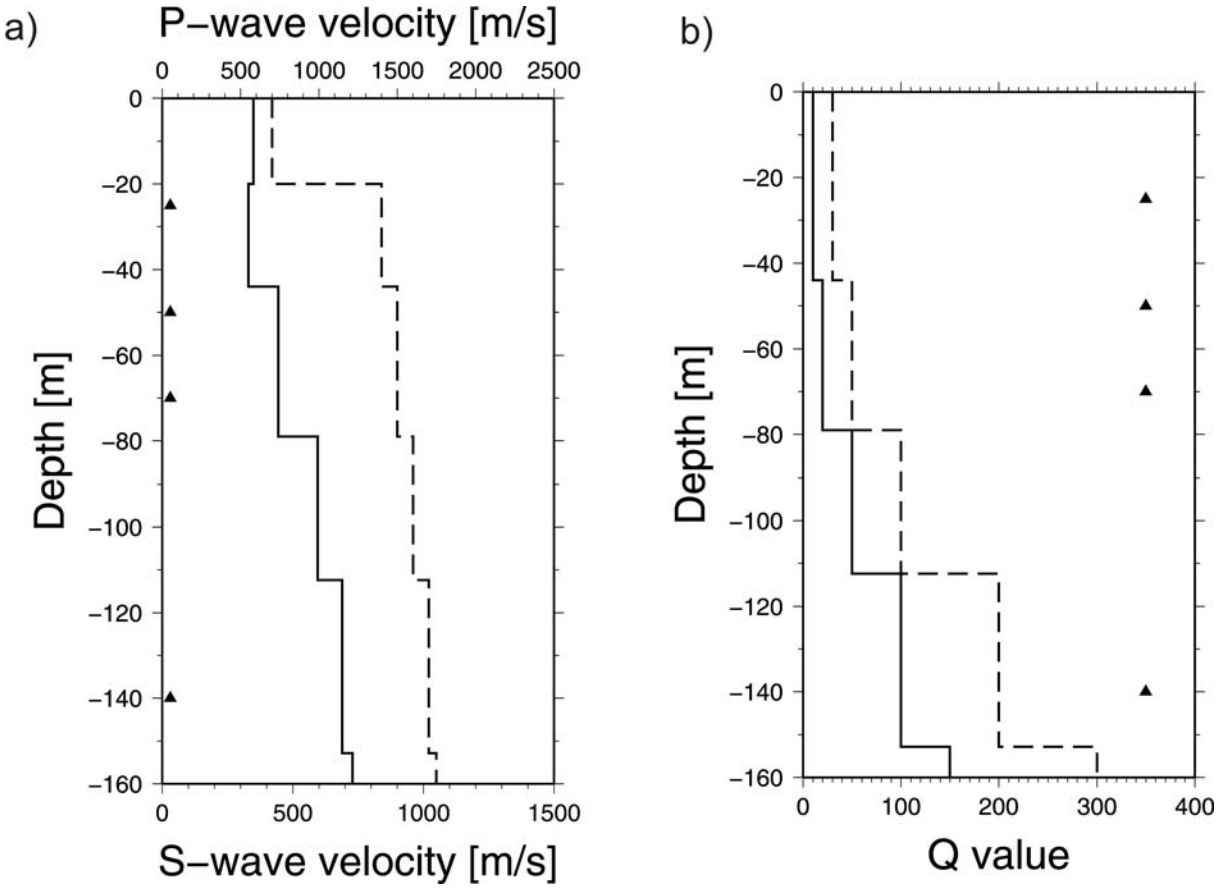

Figure 1: a) The P- (dashed line) and S-wave (continuous line) velocity profiles determined at the Ataköy vertical array by Parolai et al. (2009) used in the numerical simulations. Triangles indicate the accelerometer positions. b) The Qp (dashed line) and Qs (continuous line) variation with depth in the subsoil model used for the numerical simulations. Triangles indicate the accelerometer positions. Note that data recorded by the accelerometer installed at 25 m depth were not used in the analysis (see the text for an explanation).

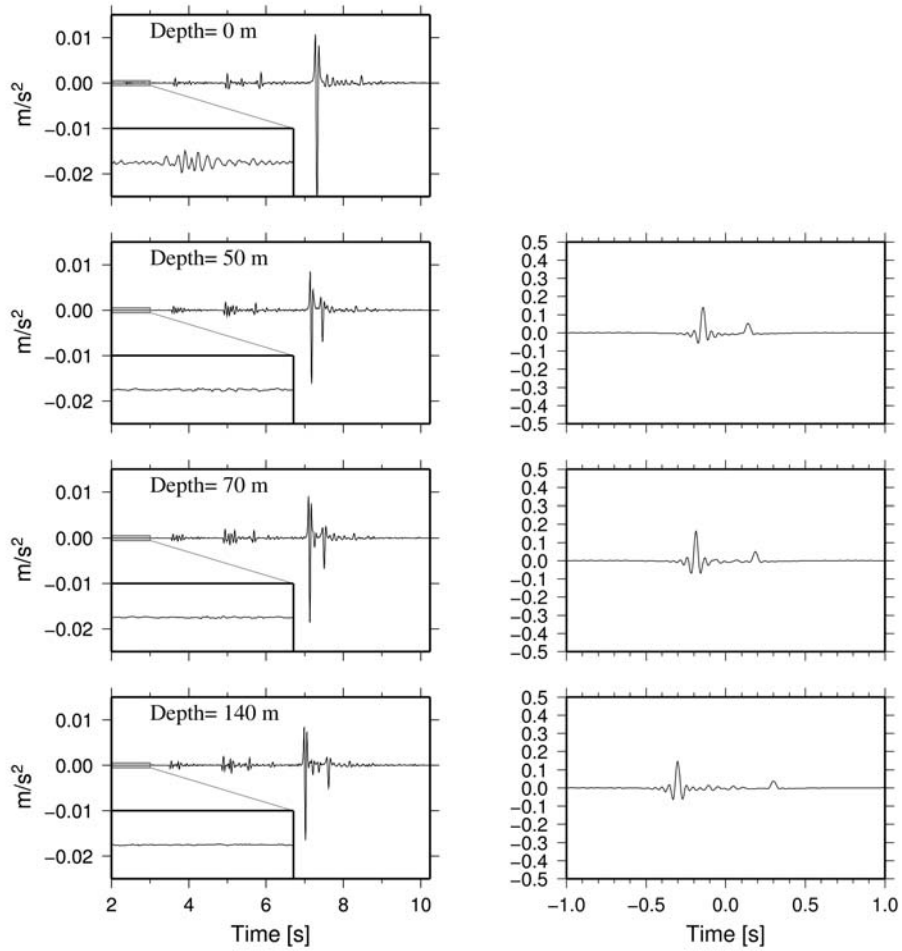

Figure 2: (Left) Synthetic maximum horizontal component accelerations for different depths (see Table 1). The insets show windows of pre-event noise in order to highlight their different amplitudes, consistent with their different depth of recording. (Right) Deconvolved wavefield for 50, 70 and 140 m depth, obtained by using equation (5).

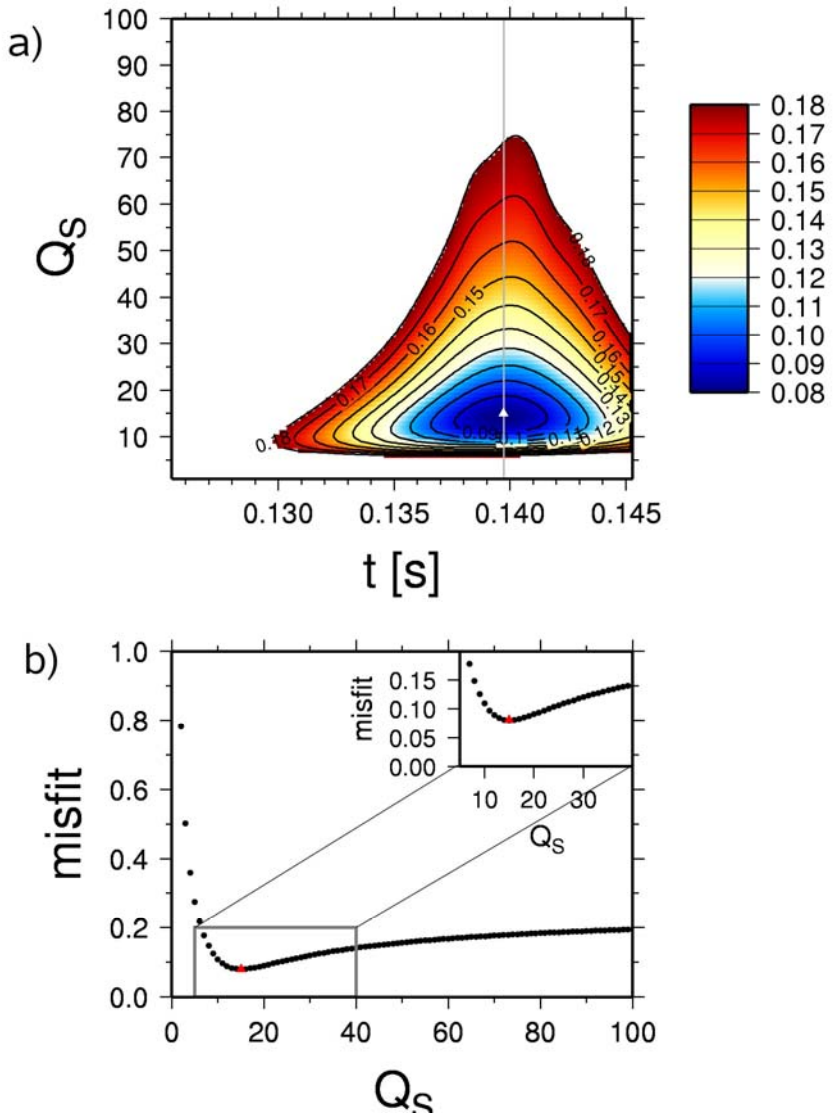

Figure 3: a) Grid search results for the depth interval 0-50 m for Method 1. The white triangle indicates the position of the minimum misfit. The gray line indicates the position of a cross-section of the misfit function passing through the global minimum. The color scale indicates the misfit values obtained with the grid search procedure. Qs values ranging between 1 and 500 with steps of 1, and τ spanning +/- two time samples around the estimated value with steps of 0.00007 sec were inverted in the grid search procedure. b) Cross-section of the misfit function (gray line in the top panel). The red triangle indicates the position of the minimum. The inset is a zoom of the area within the gray rectangle.

.

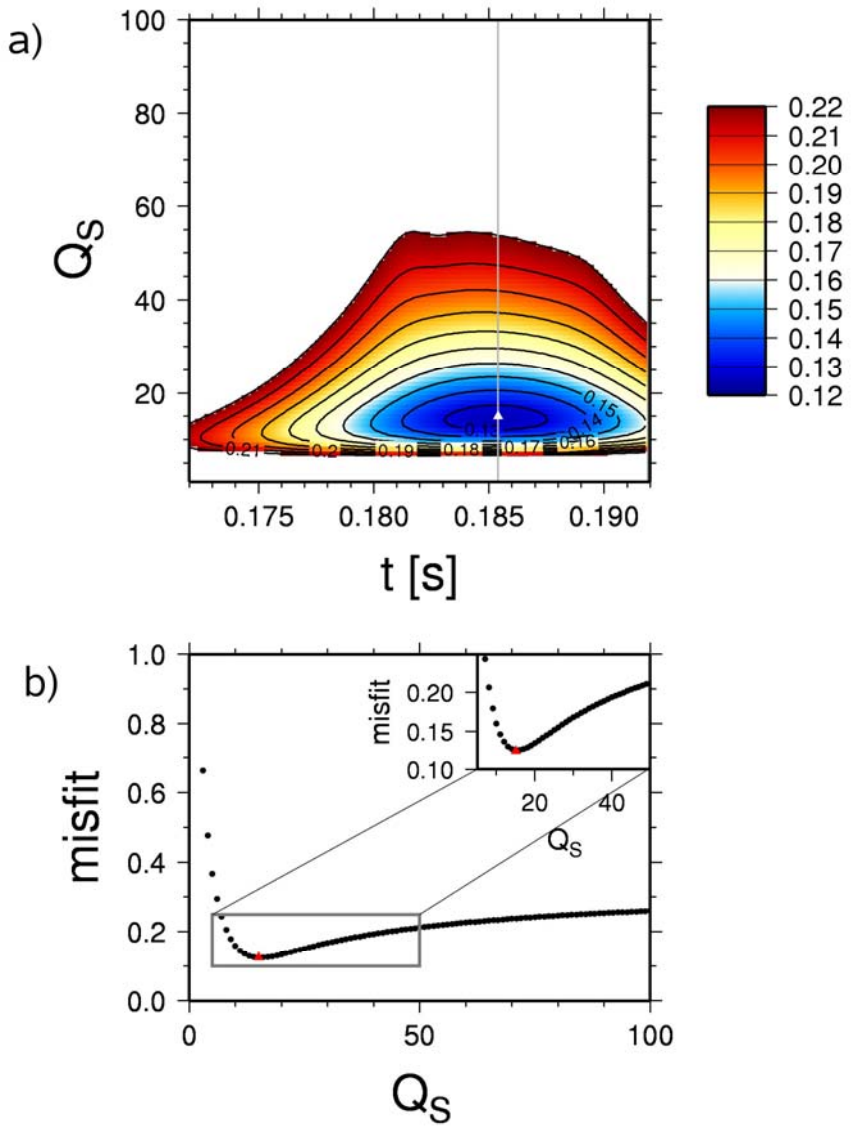

Figure 4: As in Figure 3, but for the depth interval 0-70 m.

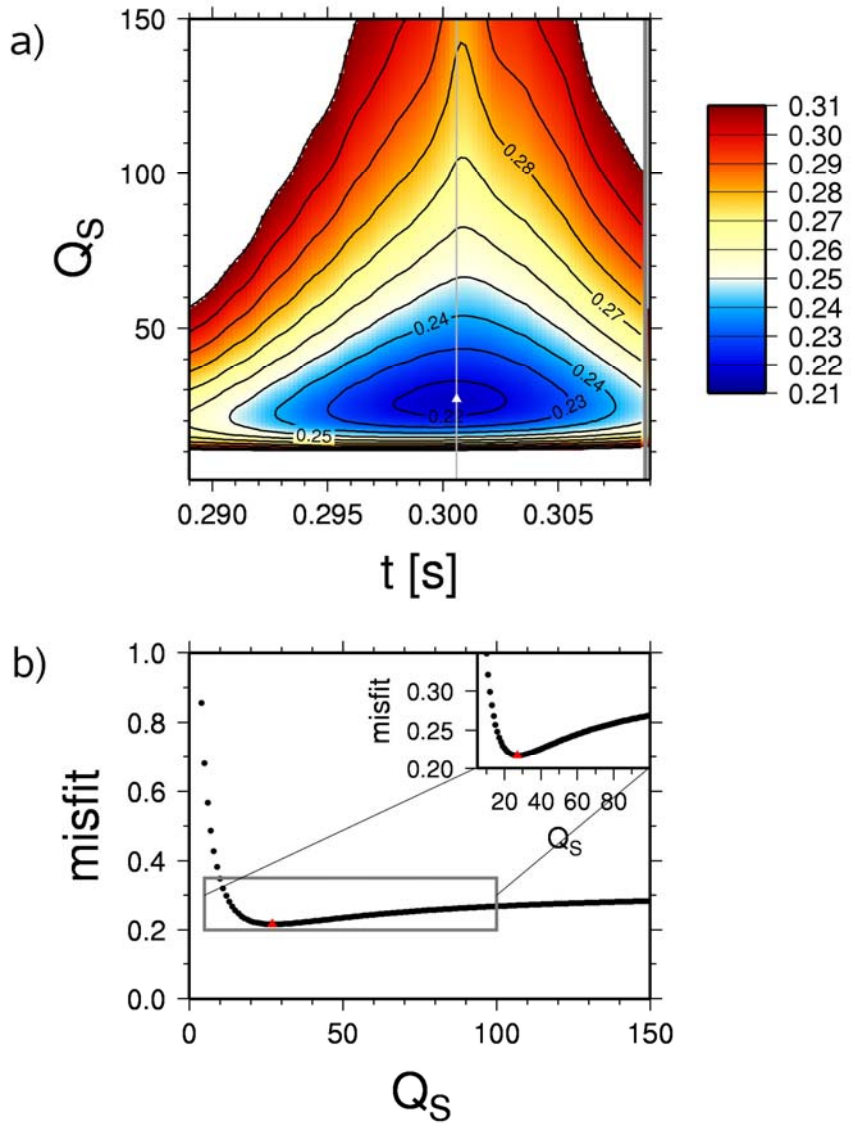

Figure 5: As in Figure 3, but for the depth interval 0-140 m.

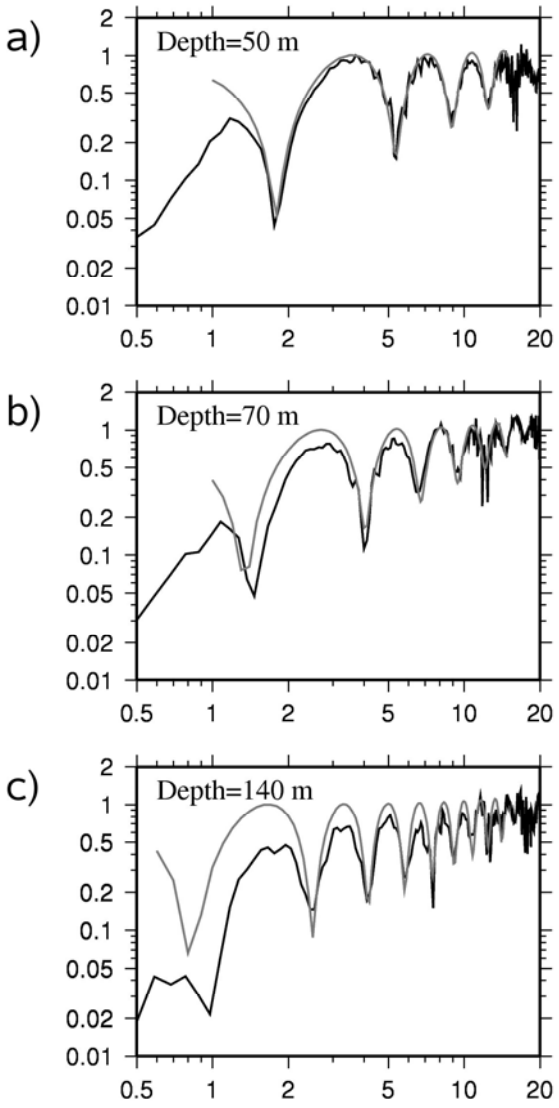

Figure 6: Synthetic acceleration deconvolved wavefield amplitude spectra (black) and calculated deconvolved wavefield spectra using the minimum misfit parameters (gray). Results are shown, from top to bottom, for the 0-50 (a), 0-70 (b) and 0-140 m (c) depth ranges.

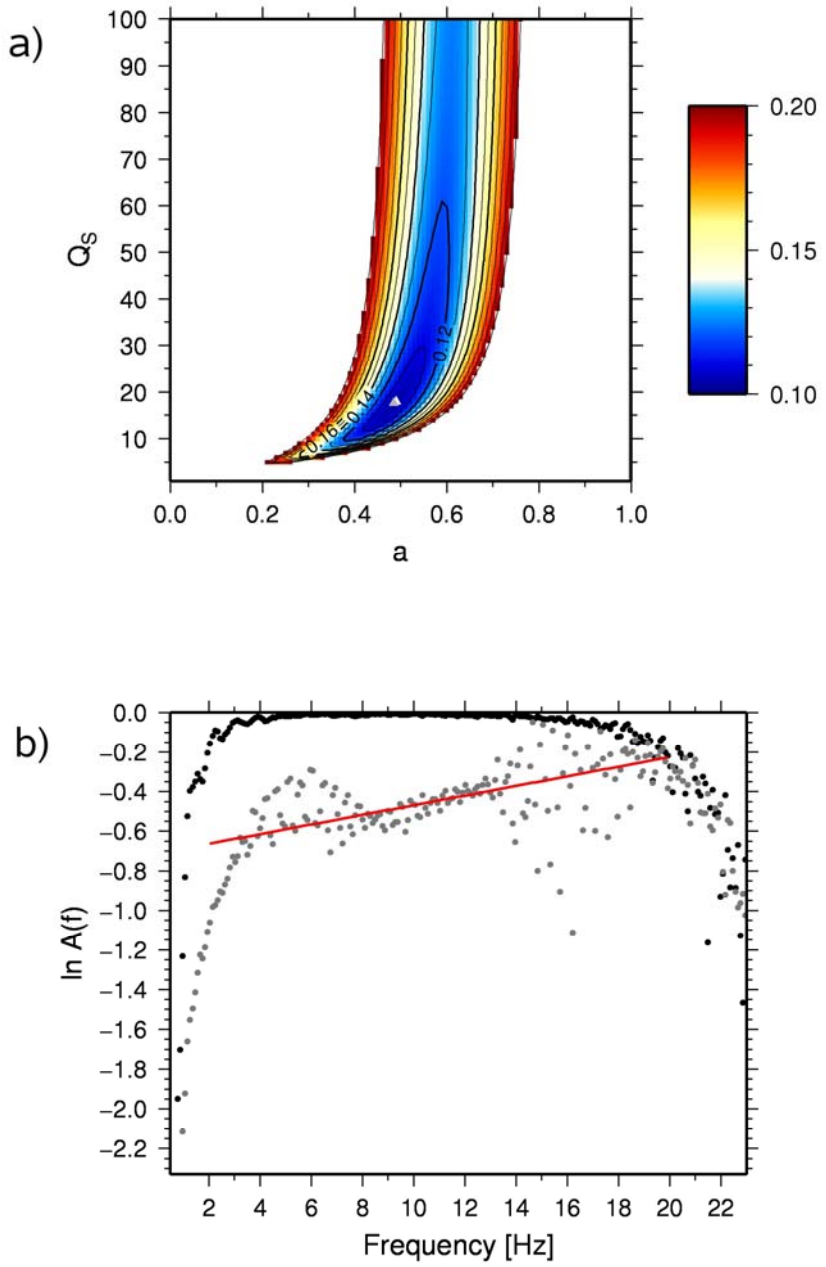

Figure 7: a) Grid search results for the depth interval 0-50 m for Method 2. The white triangle indicates the position of the minimum misfit. Qs values ranging between 1 and 500 with steps of 1, and a ranging between 0.01 and 1, with steps of 0.01 were inverted in the grid search procedure. b) Spectral amplitude of the surface wavefield deconvolved with itself (black points) and of $A(0,50;\omega)$ (gray points). The minimum misfit solution is indicated by the red line.

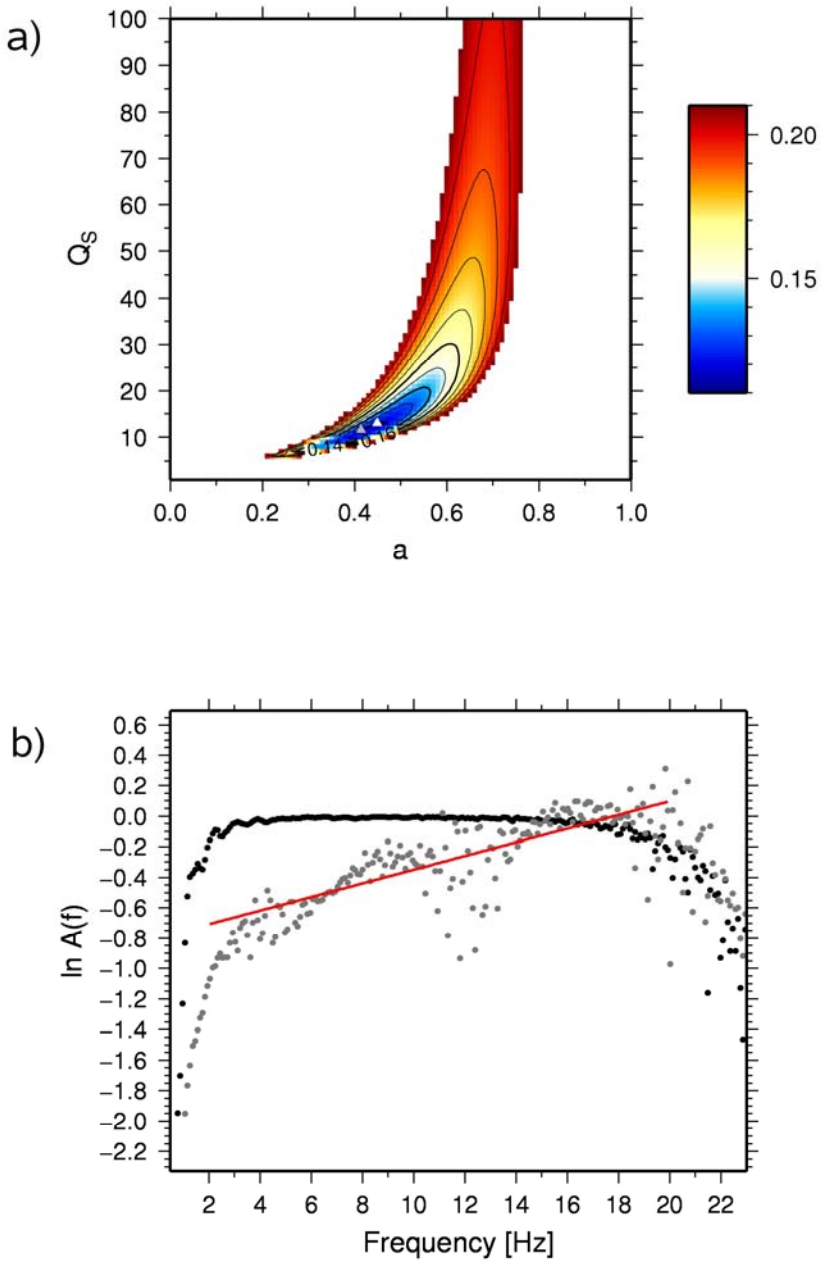

Figure 8: As in Figure 7, but for the depth range 0-70 m.

.

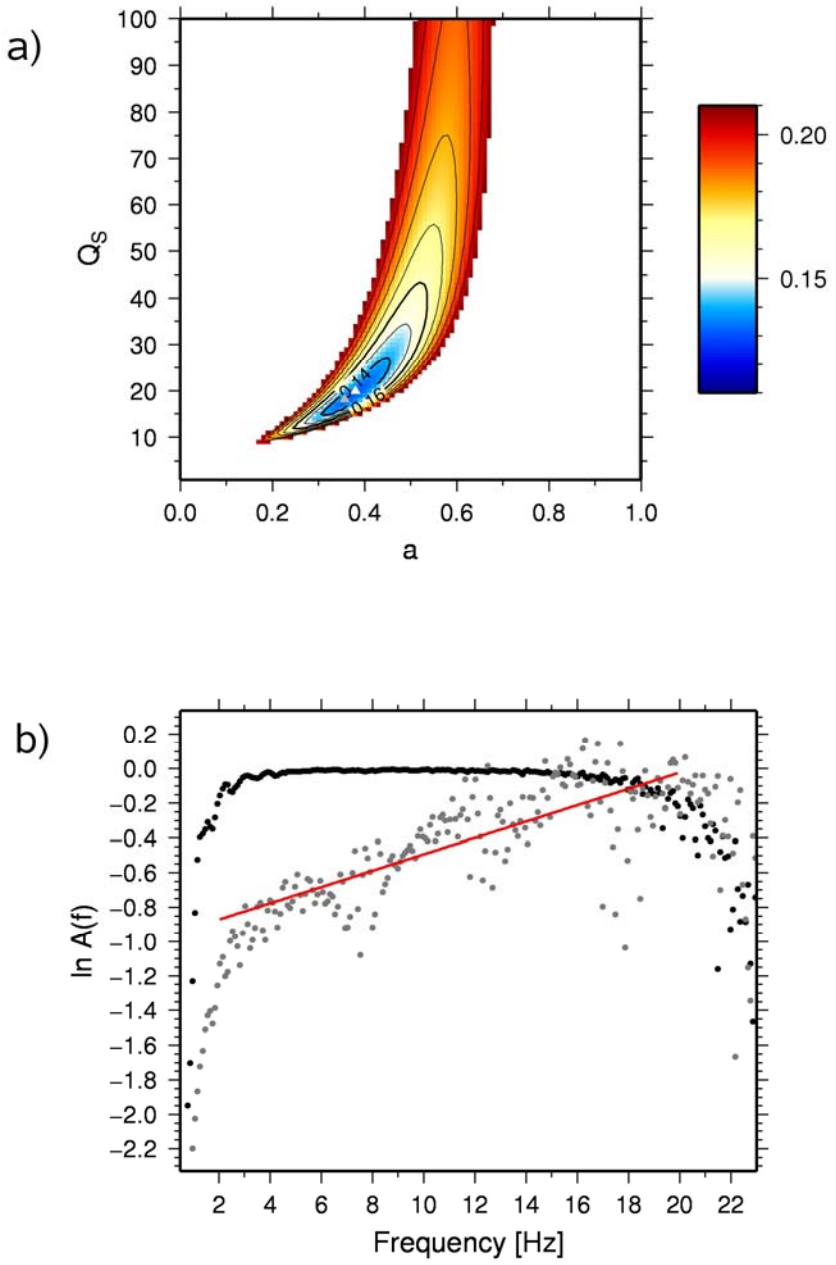

Figure 9: As in Figure 7, but for the depth range 0-140 m

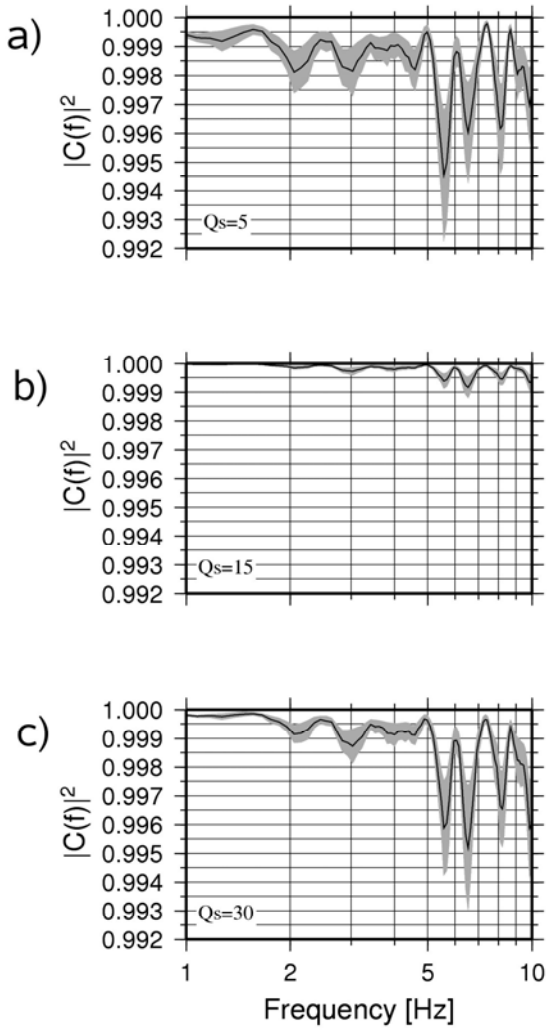

Figure 10: Multitaper squared coherency $|C(f)|^2$ estimates between the transverse component seismogram generated using the model in Table 1 and those calculated using an average Qs value (black line) over the 0-50 m depth range. The associated standard deviation uncertainties are indicated by the gray area. Results for an average Qs=5 (a), Qs=15 (b) and Qs=30 (b) are shown.

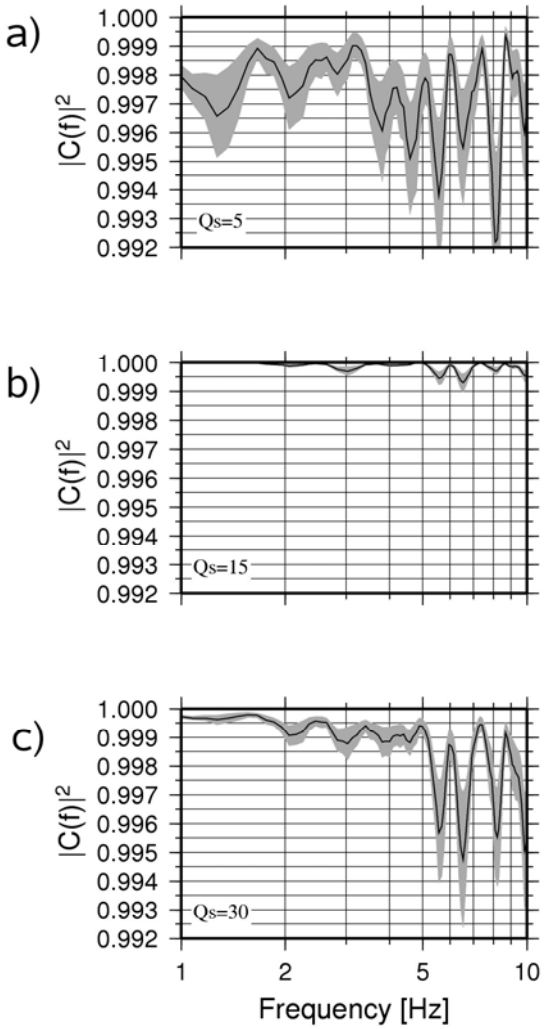

Figure 11: As in Figure 10, but for the 0-70 m depth range. The associated standard deviation uncertainties are indicated by the gray area. Results for an average Qs=5 (a), Qs=15 (b) and Qs=30 (c) are shown.

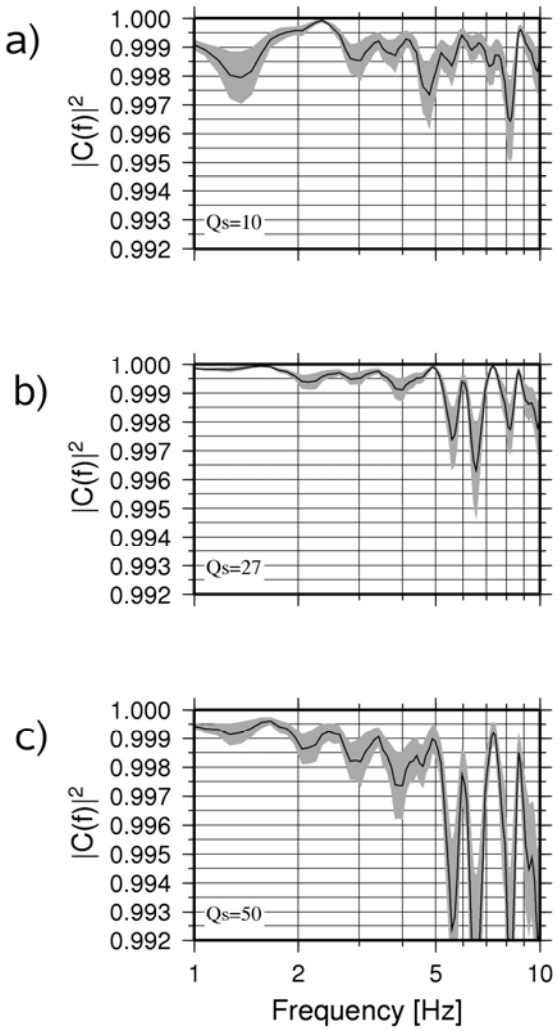

Figure 12: As in Figure 10, but for the 0-140 m depth range. The associated standard deviation uncertainties are indicated by the gray area. Results for an average Qs=10 (a), Qs=27 (b) and Qs=50 (c) are shown.

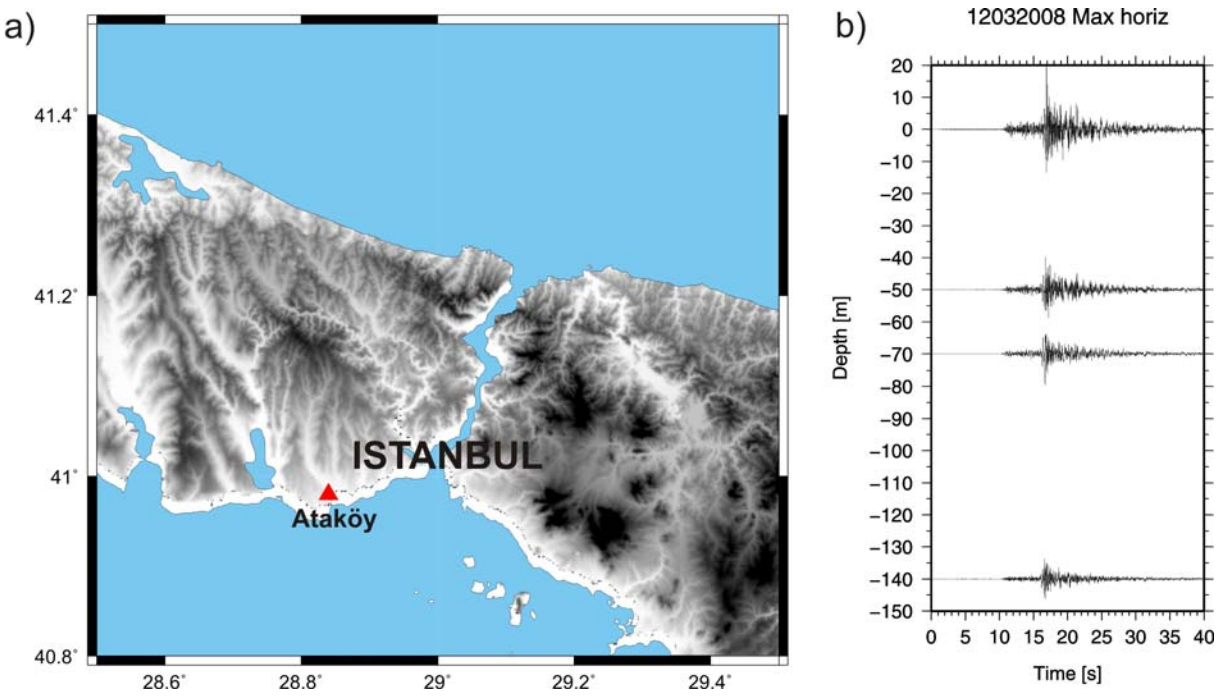

Figure 13: a) Map of the area under investigation. The triangle shows the location of the vertical array. b) Accelerometric recordings by the vertical array stations of the 18:53:38.5 March 12 2008 M=4.6 earthquake, which occurred at latitude 40.84° and longitude 28.99°. The hypocentral depth was estimated to be 10 km. More details about the recordings can be found in Parolai et al., (2009).

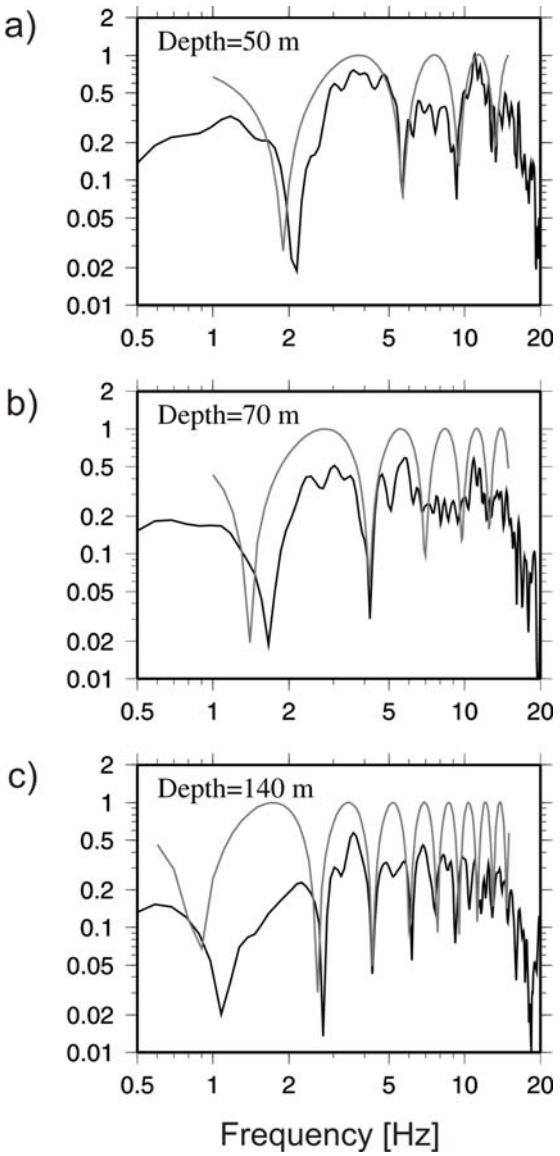

Figure 14: Observed acceleration deconvolved wavefield amplitude spectra (black) and calculated deconvolved wavefield spectra using the minimum misfit parameters (gray). Results are shown, from top to bottom, for the 0-50 m (a), 0-70 m (b) and 0-140 m (c) depth ranges.

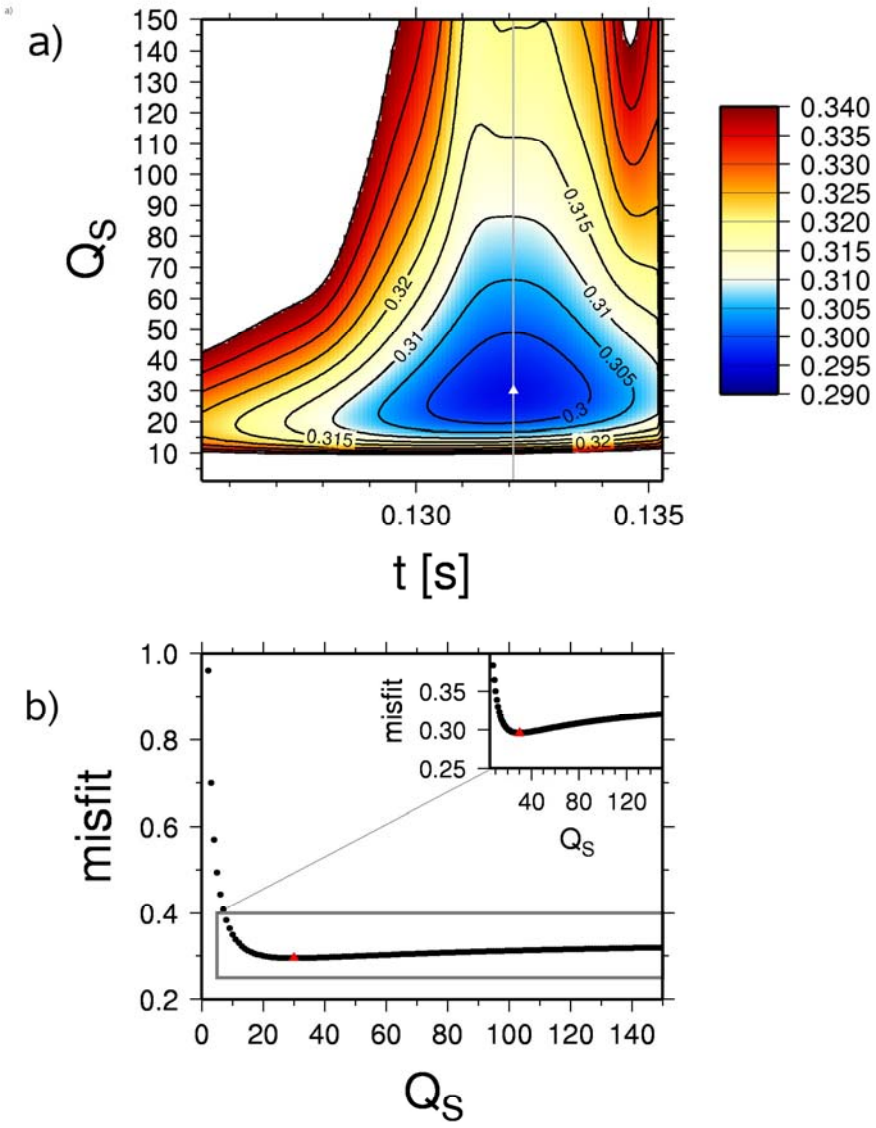

Figure 15: a) Grid search results on the observed data for the depth interval 0-50 m for Method 1. The white triangles indicate the position of the minimum misfit. The gray line indicates the position of a cross-section of the misfit function passing through the global minimum. . Qs values ranging between 1 and 500 with steps of 1, and τ spanning +/- two time samples around the estimated value with steps of 0.0002 sec were inverted in the grid search procedure .b) Cross-section of the misfit function (gray line in the top panel). The red triangle indicates the position of the minimum. The inset is a zoom of the area within the gray rectangle.

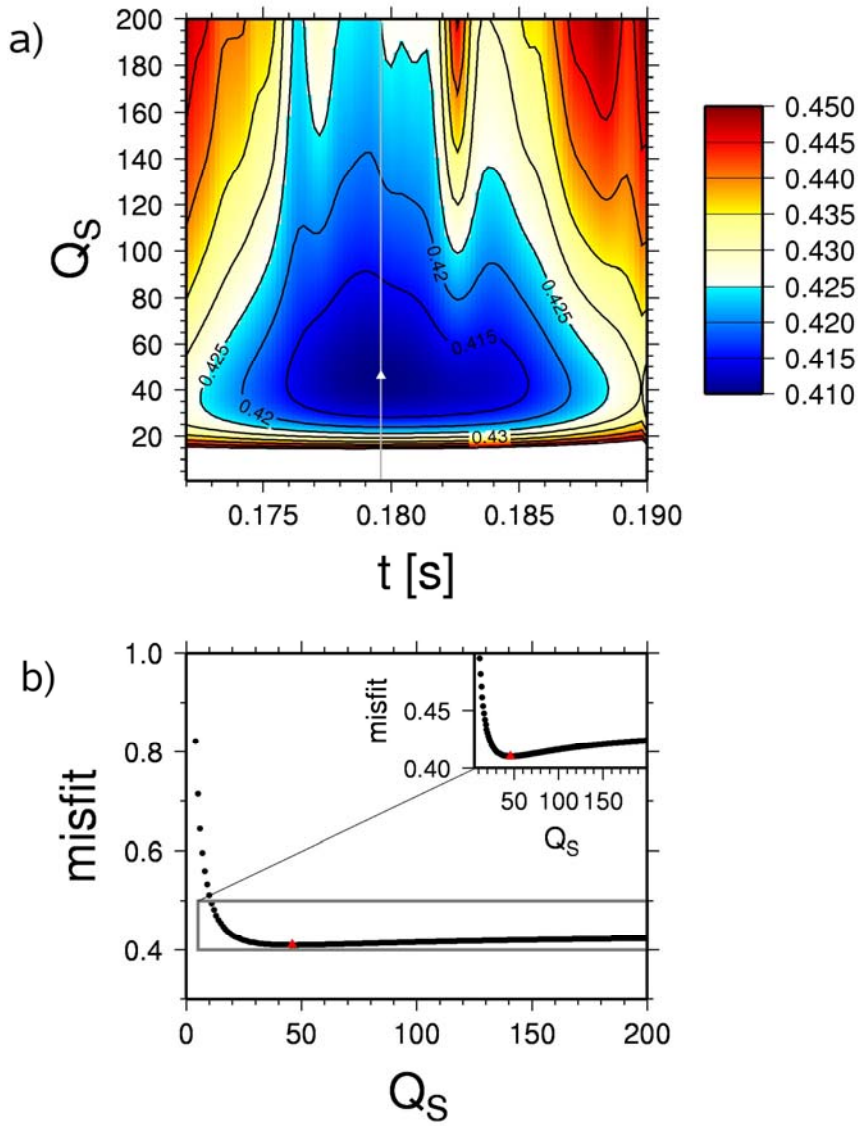

Figure 16: As in Figure15, but for the depth range 0-70 m.

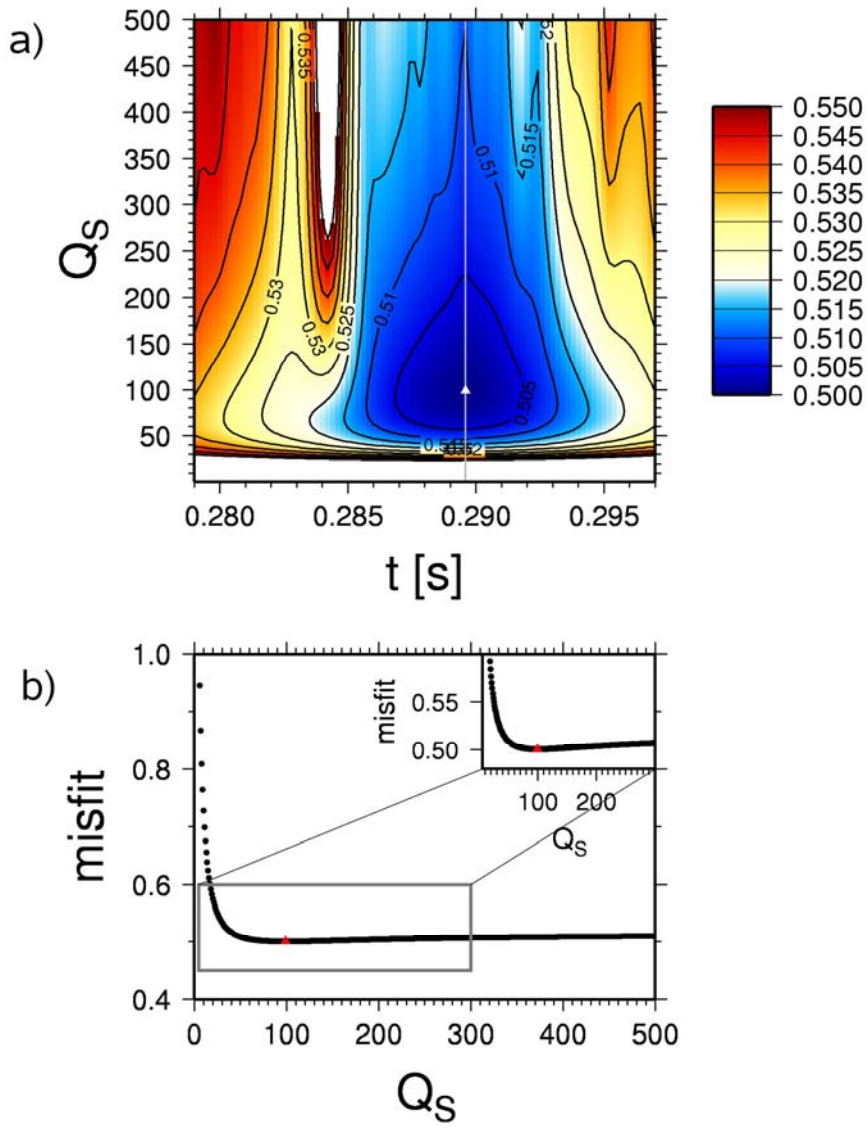

Figure 17: As in Figure15, but for the depth range 0-140 m.